Chemical Science

ROYAL SOCIETY OF CHEMISTRY

EDGE ARTICLE

View Article Online
View Journal | View Issue

Cite this: *Chem. Sci.*, 2020, **11**, 2169

All publication charges for this article have been paid for by the Royal Society of Chemistry

Received 7th November 2019
Accepted 15th January 2020

DOI: 10.1039/c9sc05643b

rsc.li/chemical-science

Multi-color tunable circularly polarized luminescence in one single AIE system†

Hongxing Shang,‡[a] Zeyang Ding,‡[a] Yue Shen,[a] Bing Yang,[a] Minghua Liu*[b] and Shimei Jiang*[a]

Circularly polarized luminescence (CPL) materials with a large luminescence dissymmetry factor (g_{lum}) and multi-color properties are very attractive. While multi-color tunable CPL can be realized by different organic dyes, the challenge of realizing both a higher g_{lum} and multiple colors using a single component remains. Here, we design an aggregation-induced emission (AIE) fluorophore, which is a pyridine functionalized cyanostilbene attached to a chiral unit, and realize multi-color tunable CPL with a high g_{lum}. The compound can self-assemble into a nanohelix and form both gel and xerogel films, exhibiting blue CPL with large g_{lum} values of -3.0×10^{-2} and -1.7×10^{-2}, respectively. With the assistance of pyridine protonation, the xerogel films exhibit red-shifted CPL signals from 480 nm to 530 nm, covering from blue *via* green and yellow to orange. Additionally, the g_{lum} remains constant during the process. This work paves a simple and convenient way to construct multi-color tunable CPL materials using a single molecule.

Introduction

Circularly polarized luminescence (CPL), a sensitive tool to reflect the chiral information in the excited state, has received widespread attention in recent years on account of its widespread potential applications in the storage of information, chemical sensors and stereoscopic displays.[1] These applications require CPL materials which exhibit a large luminescence dissymmetry factor (g_{lum}) and multi-color tunable properties in aggregates. To amplify the g_{lum}, methods like supramolecular self-assembly, energy transfer and doping of liquid crystals are utilized.[2] To realize multi-color CPL, a typical approach is to use several chiral compounds emitting different colors.[3] But tedious and complicated organic syntheses are usually needed in these processes. It remains a challenge to combine multi-color CPL with a large g_{lum} in one fluorescent dye.

To achieve this goal, we design a single molecule system and realize both higher g_{lum} and color controllable CPL in aggregates. The molecule consists of a pyridine functionalized π-structure (cyanostilbene), a chiral cholesterol group and a linking group (ester bond) and is called **Chol-CN-Py** (Fig. 1a). Firstly, the achiral cyanostilbene is a well-known aggregation-induced emission (AIE) fluorophore, which contributes to strong emission in the condensed state.[4] Besides, the negligible chirality of cholesterol in the monomer state can be amplified and transferred to the achiral fluorophore upon aggregation, leading to anticipated aggregation induced circular dichroism (AICD) and aggregation induced circularly polarized luminescence (AICPL) properties.[5] Secondly, pyridine is a well-known electronegative agent capable of protonation, which allows the change of energy

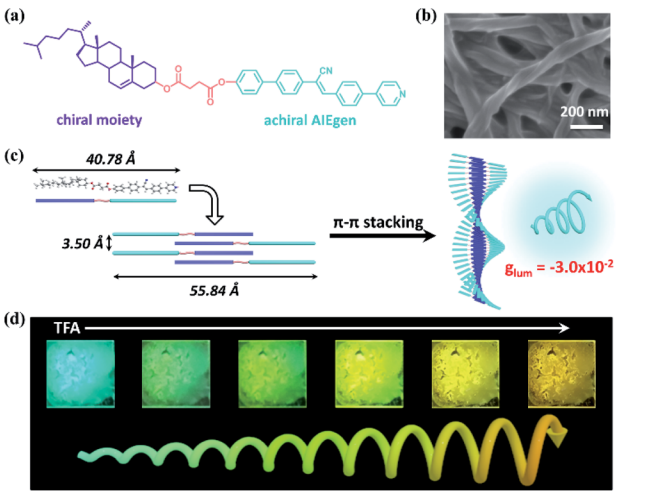

Fig. 1 (a) Chemical structure of **Chol-CN-Py**. (b) SEM image of xerogel made from DMSO. (c) Proposed molecular packing upon gel formation, leading to blue CPL. (d) Multi-color CPL upon exposure of the xerogel films to different amount of TFA.

[a]State Key Laboratory of Supramolecular Structure and Materials, College of Chemistry, Jilin University, Changchun, 130012, P. R. China. E-mail: smjiang@jlu.edu.cn

[b]CAS Key Laboratory of Colloid, Interface and Thermodynamics, Institute of Chemistry, Chinese Academy of Sciences, Beijing, 100190, P. R. China. E-mail: liumh@iccas.ac.cn

† Electronic supplementary information (ESI) available. See DOI: 10.1039/c9sc05643b

‡ These authors contributed equally to this work.

levels in the protonated state. Correspondingly, possible tunable emission as well as CPL would be realized in a single molecule system.[6]

It has been found that **Chol-CN-Py** shows great gelation ability and forms an obvious nanohelix, which allows intense blue emission and CPL in both the gel and xerogel film state. Remarkably, the g_{lum} of the gel and xerogel film are up to -3.0×10^{-2} and -1.7×10^{-2}, respectively. Under the effect of trifluoroacetic acid (TFA), the xerogel film exhibits rapid and sensitive red-shifted emission modulation owing to the equal and smooth spatial distribution and large surface area of the xerogel film.

Moreover, in the xerogel film state, the chiral structures and chirality transfer are maintained during the protonation process. Thus, through controlling the degree of protonation, the xerogel films exhibit red-shifted CPL signals from 480 nm to 530 nm, covering the multi-color circularly polarized emission from blue *via* green and yellow to orange color, with a constant handedness and g_{lum} (Fig. 1). To the best of our knowledge, this is the first multi-color tunable CPL material using a single molecule.

Results and discussion

Chol-CN-Py was synthesized by a series of Knoevenagel, Suzuki and esterification reactions as a yellow solid (Scheme S1†). The experimental details and corresponding characterization data are given in the ESI (Fig. S1–S5†). Besides, with the assistance of the synergy of van der Waals interactions and π–π interactions offered by cholesterol and the cyanostilbene group, **Chol-CN-Py** could form a stable gel in DMSO through a normal heating-cooling procedure (Table S1†).[7] The gel was also characterized by rheology experiments. The higher storage moduli (G') and the relatively low loss moduli (G'') indicated the gel formation as well as its better mechanical properties (Fig. S6†).[8]

Further characterization was performed to investigate the structure of the gel, which displayed entangled winding 3D networks consisted of left-handed nanohelix fibers, as shown in the scanning electron microscopy (SEM) images, indicating a kind of chiral expression in the microstructures (Fig. 1b and S7†).[9] Although multiple chiral centers existed in cholesterol moiety, only left-handed nanohelices were observed even in various concentrations, suggesting stable chiral self-assembly behaviors. In order to understand the packing modes, X-ray diffraction (XRD) was employed (Fig. S8†). The XRD pattern of xerogel showed four strong reflection peaks at $2\theta = 1.54°$, 3.12°, 4.71° and 6.32° in the small angle region. Based on Bragg's equation, their corresponding *d*-spacing values were calculated to be 55.84 Å, 28.10 Å, 18.74 Å and 13.97 Å, respectively, following the ratio of 1 : 1/2 : 1/3 : 1/4, indicating a layered packing structure with an interlayer distance of 55.84 Å.[10] In the wide angle region, an obvious diffraction peak with a *d*-spacing of 3.50 Å was observed, which could be assigned to the π–π stacking distance between the cyanostilbene units in the packing structures.[11] Considering that the length of the **Chol-CN-Py** molecule was only 40.78 Å, the interlayer distances of the layers were longer than the length of the molecule, but shorter than twice that. Thereby, **Chol-CN-Py** self-assembled into a bilayer structure through the π–π interactions.[12] The bilayer structure served as the basic unit and then twisted into helical nanofibers. Fibers were entangled with each other to form the chiral supramolecular gel finally. A schematic illustration is shown in Fig. 1c.

In view of the observed chiral nanohelix as well as the existence of a chiral center in the cholesterol moiety, the chirality at the ground state was probed by UV-vis absorption and CD spectra. Upon gel formation, the absorption peak exhibited a red shift in comparison to the solution, revealing that **Chol-CN-Py** adopted a J-aggregation arrangement during the self-assembly process (Fig. 2a).[13] As far as the CD spectra were concerned, the initial solution showed no signals, while in the gel state, a weak positive Cotton effect at approximately 265 nm and a strong negative Cotton effect at 393 nm were observed (Fig. 2b). Since the cholesterol-containing unit was CD silent at any wavelength longer than 350 nm, the strong Cotton effect was attributed to the chirality transfer from the cholesterol pendants to the cyanostilbene moiety upon gel formation, expressing aggregation induced circular dichroism (AICD) properties.[14]

Upon gel formation, obvious fluorescence characteristics appeared as well. In Fig. 2c, the solution containing **Chol-CN-Py** exhibited a very weak emission at 455 nm, while the emission peak red-shifted to 485 nm together with enhanced intensity in the gel state. Correspondingly, a gel with brilliant blue emission was observed. Similarly, in tetrahydrofuran (THF), consistent emission enhanced curves were observed with the addition of water (more than 60% water fraction). As for the absorption spectra, level-off tails in the visible region proved the formation of aggregates (Fig. S9†). The dynamic AIE behaviors could also be reflected during the cooling gelation process utilizing the time-dependent fluorescence spectra. The initial hot solution of **Chol-CN-Py** was almost non-emissive. Under cooling, the emission intensity increased rapidly and then remained steady

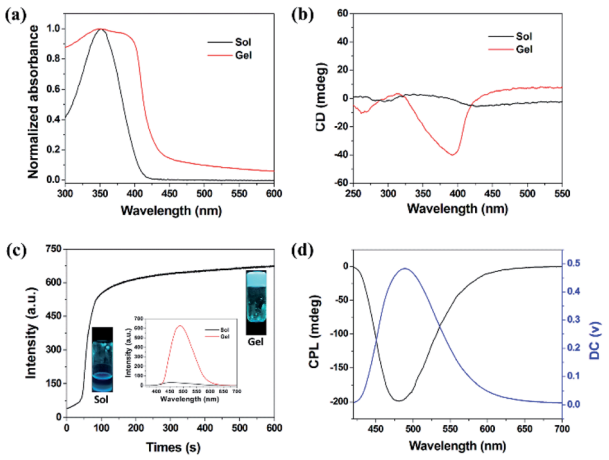

Fig. 2 (a and b) UV-vis absorption and CD spectra of the **Chol-CN-Py** solution and gel. (c) Dynamic fluorescence intensity of the **Chol-CN-Py** gel in DMSO undergoing gelation at 485 nm. Inset: the hot solution and gel fluorescence spectra (λ_{ex} = 410 nm) and fluorescence image under UV light. (d) CPL spectra of the **Chol-CN-Py** gel (λ_{ex} = 370 nm).

as observed by monitoring the intensity variation at 485 nm, indicating that the non-emissive solution completely transformed into a gel with blue emission. In addition, various photophysical data of the gel were also measured and are listed in Fig. S10† and Table 1. It is observed that the fluorescence quantum efficiency (φ_F) of the gel is up to 0.61, implying a favorable application in fluorescent materials.

According to the CD and fluorescence spectra results, the gel was not only chiral but also emissive. Thus, CPL, a unique property to evaluate the excited-state supramolecular chirality of a gel, is worth expecting in the gel state (Fig. 2d). Similar to the results of the CD spectra, no CPL signals were detected in solution. Interestingly, the gel exhibited strong right-handed CPL at 480 nm. Therefore, both ground-state and excited-state supramolecular chirality were amplified upon gel formation. Furthermore, the magnitude of CPL could be evaluated using g_{lum}, which is defined as $g_{lum} = 2(I_L - I_R)/(I_L + I_R)$, where I_L and I_R refer to the intensity of left- and right-handed CPL, respectively.[1e,15] The calculated value of g_{lum} of the CPL signals was about -3.0×10^{-2} (Fig. S11†), which was relatively large in comparison to the ones reported for most self-assembled materials.[16]

Owing to the gelation caused chirality transfer and amplification, we have obtained a **Chol-CN-Py** gel with blue CPL and a large g_{lum}. We know that CPL is sensitive to chirality and emission. If the chirality is constant, the emission regulation mechanism probably takes effect in the realization of versatile CPL. Pyridine is a functional group which can capture protons upon acid stimulus. After protonation, the enhanced electron withdrawing ability of pyridine can lead to lowered energy levels as well as red-shifted emissions.[6] TFA ($pK_a = 0.23$) with super acid can exhibit an easy and sensitive protonation effect with the pyridyl group. Thus, combining the emission modulation strategy and excited-state chirality transfer concept, we develop a multi-color CPL system by protonation.

TFA triggered protonation of **Chol-CN-Py** was characterized by ^{1}H NMR spectroscopic measurements first (Fig. S12†). With the addition of TFA, the proton peak near the pyridine nitrogen atom exhibited an obvious shift variation from 8.72 ppm to 9.02 ppm, indicating typical protonation of the pyridine unit, which further influenced the optical properties of **Chol-CN-Py**.[17] Upon TFA stimulus, gradual red-shifted absorption peaks (330–348 nm) were observed (Fig. S13†). Remarkably, in the fluorescence spectra, the initial peak with a weak blue emission red-shifted to a new one with a yellow emission ($\Delta\lambda = 85$ nm) accompanied by progressively enhanced intensity (Fig. S14†). It should be observed that the variations in ^{1}H NMR and optical features could be recovered with the assistance of triethylamine (TEA) caused deprotonation.

The process could also occur in the gel sate, which realized reversible gel–sol transitions accompanied with blue-yellow emission variations upon TFA/TEA stimuli. As shown in the fluorescence microscope and SEM images (Fig. 3), blue fibers changed to macrocrystals with yellow emission, implying the loss of the self-assembly ability after protonation. As far as the fluorescence spectra were concerned, when increasing the amount of TFA we also found obvious gradually red-shifted emission peaks (485–542 nm) (Fig. S15†). The final protonated solution showed relatively lower φ_F and shorter fluorescence lifetime in comparison with the initial gel (Fig. S16† and Table 1). The reformation of the gel and recovery of emission were realized upon TEA stimulus and the reversible variations could be repeated many times. In addition, on account of the loss of helical structures, the chiral information couldn't exist, which was reflected in the CD spectra. Upon TFA/TEA stimuli, reversible on-off CD signal transformations were detected, verifying the further change of chiral nanostructures (Fig. S17†).

To explain the optical variations, theoretical calculations for **Chol-CN-Py** and protonated **Chol-CN-Py** were employed with density functional theory (DFT) (Fig. 4). Although the HOMOs and LUMOs of **Chol-CN-Py** and protonated **Chol-CN-Py** were all localized over the cyanostilbene part, the LUMO of protonated

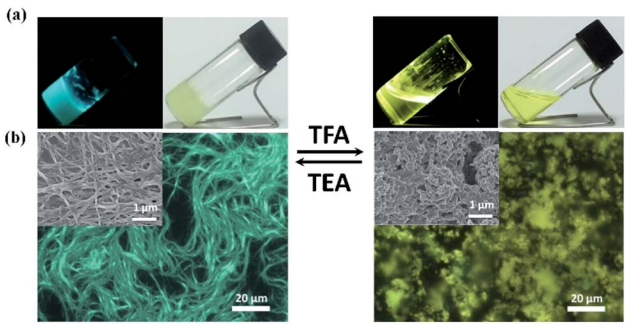

Fig. 3 (a) Photographs of the **Chol-CN-Py** gel treated with 5 equiv. TFA and TEA reversibly under UV light (left) and daylight (right). (b) Corresponding fluorescence microscope and SEM images of the gel and protonated sol.

Table 1 Emission maxima, fluorescence quantum yields, lifetimes and kinetic constants of **Chol-CN-Py** in the gel, protonated sol, film and protonated film state[a]

	λ_{em} (nm)	τ_{av} (ns)	τ_i (ns)	φ_F	k_r (ns^{-1})	k_{nr} (ns^{-1})
Gel	485	13.87	2.41 (0.03), 8.76 (0.34), 18.28 (0.63)	61%	0.0443	0.0278
Protonated sol	535	2.30	1.92 (0.99), 9.69 (0.01)	16%	0.0690	0.3658
Film	485	13.16	1.16 (0.23), 4.80 (0.48), 17.57 (0.29)	22%	0.0164	0.0595
Protonated film	550	17.18	2.17 (0.14), 8.68 (0.46), 21.63 (0.40)	32%	0.0189	0.0393

[a] λ_{em}: maximum emission wavelength; φ_F: fluorescence quantum yield determined using a calibrated integrating sphere; average lifetime: $\tau_{av} = (A_1\tau_1^2 + A_2\tau_2^2 + A_3\tau_3^2)/(A_1\tau_1 + A_2\tau_2 + A_3\tau_3)$; radiative transition rate constant: $k_r = \varphi_F/\tau_{av}$; non-radiative transition rate constant: $k_{nr} = (1 - \varphi_F)/\tau_{av}$.

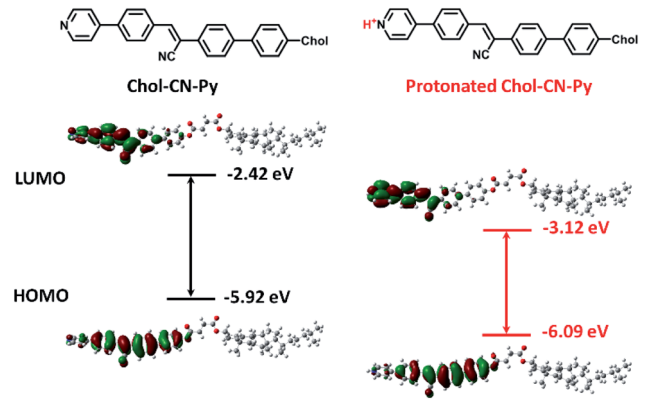

Fig. 4 The molecular structures and frontier molecular orbitals (including HOMO and LUMO energy levels) of **Chol-CN-Py** and protonated **Chol-CN-Py**.

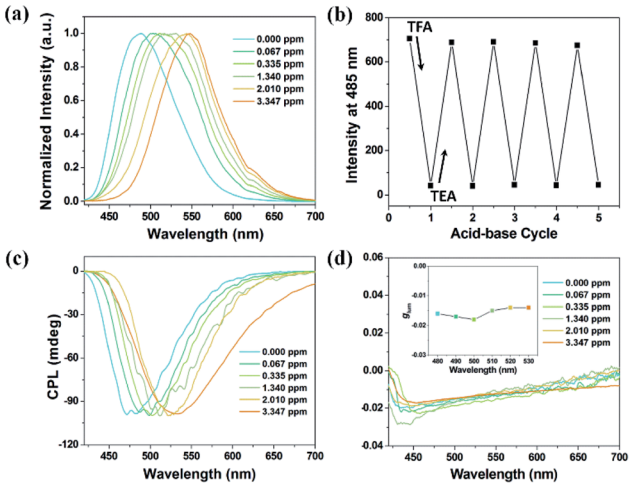

Fig. 5 (a) Normalized fluorescence of xerogel films treated with increasing amounts of TFA (0, 0.067, 0.335, 1.340, 2.010, and 3.347 ppm) for 10 s at 298 K (λ_{ex} = 410 nm). (b) The reversible switch of emission intensity of xerogel films at 485 nm by alternating TFA and TEA stimuli. (c) CPL spectra and (d) g_{lum} of xerogel films upon protonation (λ_{ex} = 370 nm).

Chol-CN-Py possessed nearer electron distribution to pyridyl hydrogen, leading to a greater decrease of LUMOs (from −2.42 eV to −3.12 eV) in comparison with HOMOs (from −5.92 eV to −6.09 eV).[18] Correspondingly, a narrower energy gap of the protonated state was reached, demonstrating the shifts of the absorption and emission to longer wavelength upon protonation.[19] In addition, the absorption spectra of both states were also calculated using time-dissolved DFT (TD-DFT) (Fig. S18†). The calculated absorption wavelengths (S_0–S_1 transition) for **Chol-CN-Py** and protonated **Chol-CN-Py** were assigned as 342.9 nm and 367.7 nm, respectively. The almost 25 nm difference was in accordance with the experimental results ($\Delta\lambda$ = 18 nm). The decreased energy gaps (from 3.62 eV to 3.37 eV) were similar to the results of HOMO and LUMO energy levels as well, implying red-shifted absorption upon protonation.

In consideration of the further application of CPL materials, films are necessary and thus xerogel films were fabricated. In particular, with the formation of the film, the aggregation state could be maintained and intense emission including CPL was expected. The hot solution containing **Chol-CN-Py** was painted onto a quartz plate to form the xerogel film to monitor the emission as well as CPL change. Upon exposure to different concentration TFA vapor, red-shifted emission peaks were observed (Fig. 5a). We also measured the detailed photophysical data for the initial and final states and found no obvious φ_F and fluorescence lifetime change, indicating outstanding stable optical properties in xerogel films during the protonation process (Fig. S19,† Table 1). It can be noted that good reversibility in the xerogel film state was also observed with alternative TEA/TFA stimuli (Fig. 5b). Additionally, the equal and smooth spatial distribution in xerogel films provided a large surface area, which made the emission modulation rapid and sensitive (Fig. S20 and S21†).[20] Upon exposure to 0.067 ppm TFA, the xerogel film with blue emission turned into one with green emission in 10 s. With the increase of the amount of TFA (0.335, 1.340, 2.010, and 3.347 ppm), a series of red-shifted xerogel films including yellow and orange were also obtained (Fig. S22†).

Simultaneously, the chiral nanostructures of the xerogel films remained constant during the TFA caused protonation process, which was demonstrated by SEM images (Fig. S23†). The chirality transfer could occur due to the stable chiral structures, leading to anticipated CPL properties. The xerogel film exhibited right-handed CPL at 480 nm and the g_{lum} was about -1.7×10^{-2}. Upon TFA stimulus, CPL signals red-shifted to 530 nm gradually, covering the multi-color circularly polarized emission from blue *via* green and yellow to orange color (Fig. 5c). In particular, the handedness and g_{lum} of CPL were almost unchanged throughout the whole course, indicating the excellent stability of the CPL xerogel films (Fig. 5d).

Conclusions

In conclusion, we developed a gel and xerogel film system which exhibited AIE as well as AICPL properties. In virtue of the gelation caused chirality transfer and amplification, both the gel and xerogel film exhibited blue CPL with a large g_{lum} (-3.0×10^{-2}, -1.7×10^{-2}). Due to the protonation of the pyridine group, reversible red-shifted emission together with gel–sol transition was realized upon TFA/TEA stimuli. In particular, in the xerogel film state, the chirality transfer and corresponding chiral structures were maintained upon protonation. In this case, by controlling the degree of protonation, the xerogel films exhibited red-shifted CPL signals from 480 nm to 530 nm, covering the multi-color circularly polarized emission from blue *via* green and yellow to orange. Meanwhile, the φ_F and g_{lum} remained constant, indicating the outstanding stability of the xerogel films. This work provides a new perspective to develop novel smart CPL tunable materials in one single system.

Conflicts of interest

There are no conflicts to declare.

Acknowledgements

This work was supported by the National Natural Science Foundation of China (51673082 and 21374036).

Notes and references

1 (*a*) J. P. Riehl and F. S. Richardson, *Chem. Rev.*, 1986, **86**, 1–16; (*b*) H. Maeda, Y. Bando, K. Shimomura, I. Yamada, M. Naito, K. Nobusawa, H. Tsumatori and T. Kawai, *J. Am. Chem. Soc.*, 2011, **133**, 9266–9269; (*c*) R. Carr, N. H. Evans and D. Parker, *Chem. Soc. Rev.*, 2012, **41**, 7673–7686; (*d*) S. T. Wu, Z. W. Cai, Q. Y. Ye, C. H. Weng, X. H. Huang, X. L. Hu, C. C. Huang and N. F. Zhuang, *Angew. Chem., Int. Ed.*, 2014, **53**, 12860–12864; (*e*) J. Han, S. Guo, H. Lu, S. Liu, Q. Zhao and W. Huang, *Adv. Opt. Mater.*, 2018, **6**, 1800538; (*f*) F. Song, Z. Xu, Q. Zhang, Z. Zhao, H. Zhang, W. Zhao, Z. Qiu, C. Qi, H. Zhang, H. H. Y. Sung, I. D. Williams, J. W. Y. Lam, Z. Zhao, A. Qin, D. Ma and B. Z. Tang, *Adv. Funct. Mater.*, 2018, **28**, 1800051; (*g*) K. Takaishi, M. Yasui and T. Ema, *J. Am. Chem. Soc.*, 2018, **140**, 5334–5338; (*h*) J. Ouyang and J. Crassous, *Coord. Chem. Rev.*, 2018, **376**, 533–547.

2 (*a*) B. A. San Jose, J. Yan and K. Akagi, *Angew. Chem., Int. Ed.*, 2014, **53**, 10641–10644; (*b*) R. Sethy, J. Kumar, R. Metivier, M. Louis, K. Nakatani, N. M. T. Mecheri, A. Subhakumari, K. G. Thomas, T. Kawai and T. Nakashima, *Angew. Chem., Int. Ed.*, 2017, **56**, 15053–15057; (*c*) Y. Wang, X. Li, F. Li, W. Y. Sun, C. Zhu and Y. Cheng, *Chem. Commun.*, 2017, **53**, 7505–7508; (*d*) D. Yang, P. Duan, L. Zhang and M. Liu, *Nat. Commun.*, 2017, **8**, 15727; (*e*) X. Li, Q. Li, Y. Wang, Y. Quan, D. Chen and Y. Cheng, *Chem.–Eur. J.*, 2018, **24**, 12607–12612; (*f*) Y. Sang, J. Han, T. Zhao, P. Duan and M. Liu, *Adv. Mater.*, 2019, 1900110; (*g*) X. Yang, J. Han, Y. Wang and P. Duan, *Chem. Sci.*, 2019, **10**, 172–178.

3 (*a*) T. Goto, Y. Okazaki, M. Ueki, Y. Kuwahara, M. Takafuji, R. Oda and H. Ihara, *Angew. Chem., Int. Ed.*, 2017, **56**, 2989–2993; (*b*) J. Han, J. You, X. Li, P. Duan and M. Liu, *Adv. Mater.*, 2017, **29**, 1606503; (*c*) H. Nishimura, K. Tanaka, Y. Morisaki, Y. Chujo, A. Wakamiya and Y. Murata, *J. Org. Chem.*, 2017, **82**, 5242–5249; (*d*) M. Li, C. Zhang, L. Fang, L. Shi, Z. Tang, H. Y. Lu and C. F. Chen, *ACS Appl. Mater. Interfaces*, 2018, **10**, 8225–8230; (*e*) N. Hellou, M. Srebro-Hooper, L. Favereau, F. Zinna, E. Caytan, L. Toupet, V. Dorcet, M. Jean, N. Vanthuyne, J. A. G. Williams, L. D. Bari, J. Autschbach and J. Crassous, *Angew. Chem., Int. Ed.*, 2017, **56**, 8236–8239; (*f*) K. Dhbaibi, L. Favereau, M. Srebro-Hooper, M. Jean, N. Vanthuyne, F. Zinna, B. Jamoussi, L. D. Bari, J. Autschbach and J. Crassous, *Chem. Sci.*, 2018, **9**, 735–742.

4 (*a*) B.-K. An, J. Gierschner and S. Y. Park, *Acc. Chem. Res.*, 2012, **45**, 544–554; (*b*) M. Martinez-Abadia, R. Gimenez and M. B. Ros, *Adv. Mater.*, 2018, **30**, 1704161; (*c*) J. Seo, J. W. Chung, J. E. Kwon and S. Y. Park, *Chem. Sci.*, 2014, **5**, 4845–4850; (*d*) H.-J. Kim, D. R. Whang, J. Gierschner and S. Y. Park, *Angew. Chem., Int. Ed.*, 2016, **55**, 15915–15919; (*e*) C. Y. Y. Yu, H. Xu, S. Ji, R. T. K. Kwok, J. W. Y. Lam, X. Li, S. Krishnan, D. Ding and B. Z. Tang, *Adv. Mater.*, 2017, **29**, 1606167; (*f*) G. Niu, X. Zheng, Z. Zhao, H. Zhang, J. Wang, X. He, Y. Chen, X. Shi, C. Ma, R. T. K. Kwok, J. W. Y. Lam, H. H. Y. Sung, I. D. Williams, K. S. Wong, P. Wang and B. Z. Tang, *J. Am. Chem. Soc.*, 2019, **141**, 15111–15120; (*g*) X. Jin, D. Yang, Y. Jiang, P. Duan and M. Liu, *Chem. Commun.*, 2018, **54**, 4513–4516.

5 (*a*) J. Liu, H. Su, L. Meng, Y. Zhao, C. Deng, J. C. Y. Ng, P. Lu, M. Faisal, J. W. Y. Lam, X. Huang, H. Wu, K. S. Wong and B. Z. Tang, *Chem. Sci.*, 2012, **3**, 2737–2747; (*b*) H. Li, S. Xue, H. Su, B. Shen, Z. Cheng, J. W. Lam, K. S. Wong, H. Wu, B. S. Li and B. Z. Tang, *Small*, 2016, **12**, 6593–6601; (*c*) J. Roose, B. Z. Tang and K. S. Wong, *Small*, 2016, **12**, 6495–6512; (*d*) H. Li, B. S. Li and B. Z. Tang, *Chem.–Asian J.*, 2019, **14**, 674–688; (*e*) H.-T. Feng, X. Gu, J. W. Y. Lam, Y.-S. Zheng and B. Z. Tang, *J. Mater. Chem. C*, 2018, **6**, 8934–8940; (*f*) Y.-X. Yuan, J.-B. Xiong, J. Luo, M. Hu, H. Jiang, M. Liu and Y.-S. Zheng, *J. Mater. Chem. C*, 2019, **7**, 8236–8243; (*g*) F. Song, Y. Cheng, Q. Liu, Z. Qiu, J. W. Y. Lam, L. Lin, F. Yang and B. Z. Tang, *Mater. Chem. Front.*, 2019, **3**, 1768–1778; (*h*) S. Zhang, J. Fan, Y. Wang, D. Li, X. Jia, Y. Yuan and Y. Cheng, *Mater. Chem. Front.*, 2019, **3**, 2066–2071.

6 (*a*) M. Kondo, S. Miura, K. Okumoto, M. Hashimoto and N. Kawatsuki, *Chem.–Asian J.*, 2014, **9**, 3188–3195; (*b*) S. Ma, J. Zhang, Y. Liu, J. Qian, B. Xu and W. Tian, *J. Phys. Chem. Lett.*, 2017, **8**, 3068–3072; (*c*) Q. Sun, H. Wang, X. Xu, Y. Lu, S. Xue, H. Zhang and W. Yang, *Dyes Pigm.*, 2018, **149**, 407–414; (*d*) J. Xiong, K. Wang, Z. Yao, B. Zou, J. Xu and X. H. Bu, *ACS Appl. Mater. Interfaces*, 2018, **10**, 5819–5827.

7 (*a*) M. Liu, G. Ouyang, D. Niu and Y. Sang, *Org. Chem. Front.*, 2018, **5**, 2885–2900; (*b*) S. Datta and S. Bhattacharya, *Soft Matter*, 2015, **11**, 1945–1953.

8 (*a*) C. D. Jones and J. W. Steed, *Chem. Soc. Rev.*, 2016, **45**, 6546–6596; (*b*) A. Dawn and H. Kumari, *Chem.–Eur. J.*, 2018, **24**, 762–776.

9 (*a*) E. Yashima, N. Ousaka, D. Taura, K. Shimomura, T. Ikai and K. Maeda, *Chem. Rev.*, 2016, **116**, 13752–13990; (*b*) L. Zhang, T. Wang, Z. Shen and M. Liu, *Adv. Mater.*, 2016, **28**, 1044–1059.

10 Y. Zhang, Y. Ma, M. Deng, H. Shang, C. Liang and S. Jiang, *Soft Matter*, 2015, **11**, 5095–5100.

11 (*a*) J. W. Liu, Y. Yang, C. F. Chen and J. T. Ma, *Langmuir*, 2010, **26**, 9040–9044; (*b*) P. Rajamalli and E. Prasad, *Org. Lett.*, 2011, **13**, 3714–3717.

12 (*a*) H. Chen, Y. Feng, G. J. Deng, Z. X. Liu, Y. M. He and Q. H. Fan, *Chem.–Eur. J.*, 2015, **21**, 11018–11028; (*b*) D. Niu, L. Ji, G. Ouyang and M. Liu, *Chem. Commun.*, 2018, **54**, 1137–1140.

13 (*a*) F. Würthner, T. E. Kaiser and C. R. Saha-Möller, *Angew. Chem., Int. Ed.*, 2011, **50**, 3376–3410; (*b*) B.-K. An, D.-S. Lee, J.-S. Lee, Y.-S. Park, H.-S. Song and S. Y. Park, *J. Am. Chem. Soc.*, 2004, **126**, 10232–10233.

14 (*a*) C. Yu, M. Xue, K. Liu, G. Wang and Y. Fang, *Langmuir*, 2014, **30**, 1257–1265; (*b*) H. Yu, Y. Lu, X. Chen, K. Liu and Y. Fang, *Soft Matter*, 2014, **10**, 9159–9166.

15 J. Kumar, T. Nakashima and T. Kawai, *J. Phys. Chem. Lett.*, 2015, **6**, 3445–3452.

16 (*a*) S. Huo, P. Duan, T. Jiao, Q. Peng and M. Liu, *Angew. Chem., Int. Ed.*, 2017, **56**, 12174–12178; (*b*) Y. Shi, P. Duan, S. Huo, Y. Li and M. Liu, *Adv. Mater.*, 2018, **30**, 1705011; (*c*) L. Ji, Y. Sang, G. Ouyang, D. Yang, P. Duan, Y. Jiang and M. Liu, *Angew. Chem., Int. Ed.*, 2019, **58**, 844–848; (*d*) J. Han, D. Yang, X. Jin, Y. Jiang, M. Liu and P. Duan, *Angew. Chem., Int. Ed.*, 2019, **58**, 7013–7019.

17 (*a*) Z. Yang, W. Qin, J. W. Y. Lam, S. Chen, H. H. Y. Sung, I. D. Williams and B. Z. Tang, *Chem. Sci.*, 2013, **4**, 3725–3730; (*b*) B. Pradhan, M. Gupta, S. K. Pal and A. S. Achalkumar, *J. Mater. Chem. C*, 2016, **4**, 9669–9673.

18 (*a*) M. J. Frisch, G. W. Trucks, H. B. Schlegel, G. E. Scuseria, M. A. Robb, J. R. Cheeseman, G. Scalmani, V. Barone, B. Mennucci, G. A. Petersson, H. Nakatsuji, M. Caricato, X. Li, H. P. Hratchian, A. F. Izmaylov, J. Bloino, G. Zheng, J. L. Sonnenberg, M. Hada, M. Ehara, K. Toyota, R. Fukuda, J. Hasegawa, M. Ishida, T. Nakajima, Y. Honda, O. Kitao, H. Nakai, T. Vreven, J. A. Montgomery Jr, J. E. Peralta, F. Ogliaro, M. Bearpark, J. J. Heyd, E. Brothers, K. N. Kudin, V. N. Staroverov, R. Kobayashi, J. Normand, K. Raghavachari, A. Rendell, J. C. Burant, S. S. Iyengar, J. Tomasi, M. Cossi, N. Rega, J. M. Millam, M. Klene, J. E. Knox, J. B. Cross, V. Bakken, C. Adamo, J. Jaramillo, R. Gomperts, R. E. Stratmann, O. Yazyev, A. J. Austin, R. Cammi, C. Pomelli, J. W. Ochterski, R. L. Martin, K. Morokuma, V. G. Zakrzewski, G. A. Voth, P. Salvador, J. J. Dannenberg, S. Dapprich, A. D. Daniels, Ö. Farkas, J. B. Foresman, J. V. Ortiz, J. Cioslowski and D. J. Fox, *Gaussian 09 Revision D.01*, Gaussian Inc., Wallingford CT, 2009; (*b*) W. Li, P.-P. Yang, L. Wang and H. Wang, *J. Mater. Chem. C*, 2015, **3**, 3783–3789.

19 (*a*) X. Chen, X. Y. Shen, E. Guan, Y. Liu, A. Qin, J. Z. Sun and B. Z. Tang, *Chem. Commun.*, 2013, **49**, 1503–1505; (*b*) S. Huang, Y. Wu, F. Zeng, L. Sun and S. Wu, *J. Mater. Chem. C*, 2016, **4**, 10105–10110.

20 (*a*) K. K. Kartha, S. S. Babu, S. Srinivasan and A. Ajayaghosh, *J. Am. Chem. Soc.*, 2012, **134**, 4834–4841; (*b*) H. Wang, J. Zhao, G. Yang, F. Zhang, J. Sun and R. Lu, *Org. Biomol. Chem.*, 2018, **16**, 2114–2124; (*c*) Y. Ma, M. Cametti, Z. Džolić and S. Jiang, *J. Mater. Chem. C*, 2018, **6**, 9232–9237.